ON THE MINIMUM CORE MASS FOR GIANT PLANET FORMATION

Ana-Maria A. Piso
Harvard-Smithsonian Center for Astrophysics

Andrew N. Youdin
JILA, University of Colorado at Boulder
Draft version October 3, 2013

ABSTRACT

1. INTRODUCTION

Current theories of giant planet formation postulate that these planets form either through core accretion or gravitational instability (GI). In the core accretion model (e.g., Harris 1978, Mizuno et al. 1978, Stevenson 1982, Bodenheimer & Pollack 1986, Wuchterl 1993, Pollack et al. 1996, D'Angelo et al. 2011), solid planetesimals collide and grow into a massive solid core which then accretes a gaseous envelope. GI theories postulate that giant planets can be formed due to the fragmentation of the protoplanetary disk into self-gravitating clumps (e.g., Harris 1978, Boss 1997, Rafikov 2005, Kratter et al. 2010, D'Angelo et al. 2011).

Forming giant planets at wide separations in the protoplanetary disk poses theoretical challenges. Even though GI works better at large distances than in the inner disk (e.g., Rafikov 2005), fine-tuning is still required in terms of disk conditions and infall history for planetary mass objects to be the outcome of GI (Kratter et al. 2010). On the other hand, core accretion times are thought to be too long in the outer disk, largely due to the time it takes to accrete the solid core. Some models, however, allow for rapid accretion of solids even at large separations (e.g., Dones & Tremaine 1993, Kenyon & Bromley 2009, Lambrechts & Johansen 2012). We thus consider the timescale constraints imposed by the accretion of the gaseous atmosphere before the protoplanetary disk dissipates.

Several types of core accretion models have been studied previously. In static models, which are mostly analytic, the accretion rate of planetesimals regulates the growth of the atmosphere (e.g., Stevenson 1982, Rafikov 2006). The luminosity of the gaseous envelope is thus entirely supplied by planetesimal accretion. These studies consider that the atmosphere is in a steady state at all times, in which all the incoming energy from planetesimal accretion is radiated away by the envelope. For a fixed planetesimal accretion rate, the atmosphere mass grows non-linearly as the core mass increases. As the atmosphere mass becomes comparable to the mass of the solid core, hydrostatic balance no longer holds and the static model breaks down. Unstable collapse occurs if the core mass further increases, a process known as the "core accretion instability". The maximum core mass for which the atmosphere is still in hydrostatic equilibrium is defined as the "critical core mass". Typically, the critical core mass is found to be about $10M_\oplus$ (e.g., Stevenson 1982, Rafikov 2006).

Full time dependent simulations of giant planet evolution take into account the Kelvin-Helmholtz (KH) contraction of the gaseous envelope. As a result, the atmosphere is no longer in a steady state, but rather it accretes gas as it cools radiatively. These evolutionary models for core and atmosphere growth allow for the planetesimal accretion rate to be directly calculated as a function of time rather than prescribed, as it is the case in the static models. Pollack et al. (1996) find that the planet growth can be separated into three relatively well defined phases. Phase 1 is dominated by the growth of the core due to runaway planetesimal accretion, and ends when the planet's feeding zone has been depleted of solids. At this stage, planetesimal accretion can no longer balance radiative losses, and the atmosphere cools and contracts. This is phase 2, during which the envelope mass steadily increases, while core growth is no longer significant. Once the atmosphere mass becomes comparable to the core mass, growth is continually accelerated, leading to runaway gas accretion, i.e. phase 3. Phase 2 is found to be much longer than the other two phases (see also Alibert et al. 2005), hence the evolutionary timescale of the atmosphere is set by KH contraction.

Since KH contraction dominates the envelope accretion timescale in many core accretion models, it is useful to study atmospheric growth onto a core of fixed mass (Ikoma et al. 2000, Papaloizou & Nelson 2005). This regime is considered in this work. We explore the atmosphere evolution around fully grown cores of different masses, and determine the minimum core mass needed to form a giant planet before disk dissipation for a variety of disk conditions and properties of the nebular gas. We note that our models are a special case of the time dependent studies, with the planetesimal accretion rate set to zero.

This paper is organized as follows. In section §2 we describe the assumptions of our atmosphere model, and derive the basic equations that govern the structure and evolution of the atmosphere. In section §3, we present a simplified analytic model that predicts the qualitative behavior of the numerical model. We describe our numerical results in section §4, and determine the critical core mass for planet formation during the life time of the protoplanetary disk in section §5. We discuss some of the approximations of our model in section §6 and summarize our findings in section §7.

2. ATMOSPHERE MODELS

To model the growth of planetary atmospheres around a solid core, we develop a simplified two layer model for time-dependent atmospheric cooling, i.e. Kelvin-Helmholtz (KH) contraction. With a convective interior and radiative exterior, this model is motivated by similar models of hot Jupiters (Arras & Bildsten 2006; Youdin & Mitchell 2010).

Our model can accurately model the growth of the atmosphere up to the crossover mass, when the atmosphere mass equals the mass of the core. Beyond the crossover mass, our approximate treatment of the radiative zone (explained below) breaks down. Since subsequent growth is a rapid runaway process (e.g., Pollack et al. 1996), our model can investigate to good accuracy the timescale requirement of core accretion. Our simplified treatment is also inappropriate for hot, short-period planets, where dust sublimation gives deeper radiative zones that require more detailed models.

Our main assumptions are summarized as follows:

1. The atmosphere is spherically symmetric and remains in hydrostatic balance during its thermal evolution.

2. The core mass and radius are fixed in evolutionary calculations, neglecting ongoing planetesimal or dust accretion.

3. At the planet's Hill radius, the atmospheric temperature and pressure match the conditions of the disk midplane.

4. The only source of planetary luminosity is the gravitational contraction of the atmosphere.

5. In the radiative zone, luminosity generation is neglected, i.e. the luminosity is held constant.

6. A global cooling model connects independent static solutions into a time-dependent sequence.

7. A polytropic EOS is assumed for simplicity.

8. Dust grains provide the opacity in the radiative zone, which remains cool enough to avoid dust sublimation.

9. Because gas accretion accelerates after the crossover mass, the time to reach the crossover mass, i.e. the crossover time, is a good approximation of the total time to form a gas giant.

The remainder of this section develops our model in more detail.

2.1. Disk and Opacity Model

We adopt a minimum mass solar nebula (MMSN) model for a passively irradiated disk (Chiang & Youdin 2010). With the semi-major axis a normalized to the outer disk as $a_{10} = a/(10 \text{ AU})$, the gas surface density and mid-plane temperature are

$$\Sigma_{\rm d} \;=\; 70\, F_\Sigma a_{10}^{-3/2} \text{ g cm}^{-2} \tag{1a}$$

$$T_{\rm d} \;=\; 45\, F_T\, a_{10}^{-3/7} \text{ K}. \tag{1b}$$

The normalization factors F_Σ and F_T adjust the model relative to the fiducial MMSN. We fix $F_\Sigma = F_T = 1$ unless noted otherwise.

For a vertically isothermal disk in hydrostatic balance (with no self-gravity), the mid-plane pressure of disk gas is

$$P_{\rm d} = 6.9 \times 10^{-3} F_\Sigma \sqrt{F_T}\, a_{10}^{-45/14} \text{ dyne cm}^2 \tag{2}$$

for a molecular weight of $\mu = 2.35$ proton masses and a Solar mass star.

The (thermodynamically isothermal) sound speed in the disk is

$$c_{\rm d} = \sqrt{\mathcal{R} T_{\rm d}} = 0.4 \sqrt{F_T} a_{10}^{3/14} \text{ km s}^{-1} \tag{3}$$

in terms of the specific gas constant $\mathcal{R}$. The disk scale-height is

$$H_{\rm d} = c_{\rm d}/\Omega = 0.42 \sqrt{F_T}\, a_{10}^{9/7} \text{ AU}. \tag{4}$$

in terms of the Keplerian frequency $\Omega = \sqrt{GM_*/a^3}$ with G the gravitational constant and M_* the stellar (in this work Solar) mass.

We assume a dust opacity following Bell & Lin (1994):

$$\kappa = 2 F_\kappa \left(\frac{T}{100 \text{ K}} \right)^\beta \text{ cm}^2 \text{ g}^{-1}, \tag{5}$$

with a powerlaw index $\beta = 2$ and normalization $F_\kappa = 1$ unless noted otherwise. Grain growth tends to lower both F_κ and β, while dust abundance scales with F_κ. Section ?? discusses dust sublimation and more realistic opacity laws.

2.2. Length Scales

The characteristic length scales for protoplanetary atmospheres are crucial for choosing boundary conditions and for understanding the validity of spherical symmetry in a disk of scaleheight $H_{\rm d}$. The radius of the solid core:

$$R_{\rm c} \equiv \left(\frac{3M_{\rm c}}{4\pi \rho_{\rm c}} \right)^{1/3} \approx 10^{-4} m_{\rm c10}^{1/3} \text{ AU}, \tag{6}$$

where the core mass, $M_{\rm c}$, is normalized to 10 Earth masses as $m_{\rm c10} \equiv M_{\rm c}/(10\, M_\oplus)$. The core density is held fixed at $\rho_{\rm c} = 3.2$ g cm^{-3}. We thus neglect the detailed equation of state of the solid core (Fortney et al. 2007).

A planet can bind a dense atmosphere if its escape speed exceeds the sound speed. This criterion is satisfied inside the Bondi radius

$$R_{\rm B} \equiv \frac{GM_{\rm p}}{c_{\rm d}^2} \approx 0.17 \frac{m_{\rm p10}\, a_{10}^{3/7}}{F_T} \text{ AU} \tag{7}$$

where the enclosed planet mass, $M_{\rm p} = M_{\rm c} + M_{\rm atm}$, includes the core and any atmosphere within the Bondi radius. The scalings thus use $m_{\rm p10} \equiv M_{\rm p}/(10\, M_\oplus)$.

Stellar tides dominate the planet's gravity beyond the Hill radius

$$R_{\rm H} = \left(\frac{M_{\rm p}}{3M_*} \right)^{1/3} a \approx 0.22\, m_{\rm p10}^{1/3} a_{10} \text{ AU} \tag{8}$$

where hydrostatic balance breaks down. In Equation (8), $M_{\rm p}$ includes mass enclosed within $R_{\rm H}$. During the early

stages of evolution, $M_{\rm p} \sim M_{\rm c}$, and the core mass can be used to get estimates of both $R_{\rm B}$ and $R_{\rm H}$.

The relevant length scales of the atmosphere and disk satisfy the relation $R_{\rm B} H_{\rm d}^2 = 3 R_{\rm H}^3$. The lengthscales are roughly equal at the "thermal mass" (e.g., Menou & Goodman 2004)

$$M_{\rm th} > \frac{c_{\rm d}^3}{G\Omega} \approx 25 \, \frac{F_T^{3/2}}{\sqrt{m_*}} \, a_{10}^{6/7} \, M_\oplus \,. \qquad (9)$$

In the low mass regime, $M_{\rm p} < M_{\rm th}/\sqrt{3}$, the lengthscales order as $R_{\rm B} < R_{\rm H} < H_{\rm d}$ (R06). In this regime, many studies assume the atmosphere matches the disk conditions at $R_{\rm B}$. We however use $R_{\rm H}$ as the matching radius in both this low mass and other higher mass regimes. This choice is justified by the fact that, for hydrostatic solutions, the density at $R_{\rm B}$ exceeds the disk's background density by an order unity factor (R06). This modest density change has a similarly modest effect on our results.

For a finite range of intermediate masses, $M_{\rm th}/\sqrt{3} < M_{\rm p} < 3 M_{\rm th}$, the Hill radius is the smallest scale, satisfying both $R_{\rm H} < R_{\rm B}$ and $R_{\rm H} < H_{\rm d}$. Spherical symmetry remains a good, if imperfect, approximation because the disk is only weakly vertically stratified on scales $\lesssim H_{\rm d}$.

At higher planet masses where $M_{\rm p} > 3 M_{\rm th}$ and $H_{\rm d} < R_{\rm H} < R_{\rm B}$, spherical symmetry is no longer a good approximation, due to both the vertical stratification of the disk and gap opening. See §6.1 for discussion of neglected non-hydrostatic effects on all mass scales.

Note that while $R_{\rm H}$ is the outer boundary of our structure calculations, we define planet masses to include only the mass inside the smaller of $R_{\rm B}$ or $R_{\rm H}$. This conservative choice in quoting planet masses is usually a minor distinction because (when $R_{\rm B} < R_{\rm H}$) the gas between $R_{\rm B}$ and $R_{\rm H}$ is weakly compressed.

2.3. Structure Equations and Boundary Conditions

Our atmosphere calculations use the standard structure equations of mass conservation, hydrostatic balance, thermal gradients, and energy conservation:

$$\frac{dm}{dr} = 4\pi r^2 \rho \qquad (10a)$$

$$\frac{dP}{dr} = -\frac{Gm}{r^2}\rho \qquad (10b)$$

$$\frac{dT}{dr} = \nabla \frac{T}{P}\frac{dP}{dr} \qquad (10c)$$

$$\frac{dL}{dr} = 4\pi r^2 \rho \left(\epsilon - T\frac{\partial S}{\partial t}\Big|_m \right), \qquad (10d)$$

where r is the radial coordinate, P, T, ρ and L are the gas pressure, temperature, density and luminosity, respectively. The enclosed mass at radius r is m. Equation (10c) simply defines the temperature gradient $\nabla \equiv d\ln T/d\ln P$. In radiative zones radiative diffusion gives a temperature gradient

$$\nabla_{\rm rad} \equiv \frac{3\kappa P}{64\pi Gm\sigma T^4}L, \qquad (11)$$

where σ is the Stefan-Boltzmann constant. In convectively unstable regions, efficient convection gives an isen-

tropic temperature gradient with $\nabla = \nabla_{\rm ad}$, the adiabatic gradient

$$\nabla_{\rm ad} \equiv \left(\frac{d\ln T}{d\ln P}\right)_{\rm ad} \qquad (12)$$

According to the Schwarzschild criterion, convective instability occurs when $\nabla_{\rm rad} > \nabla_{\rm ad}$. Thus $\nabla = \min(\nabla_{\rm rad}, \nabla_{\rm ad})$ sets the temperature gradient.

In the energy equation (10d), ϵ represents all local sources of heat input, which excludes the motion of the atmosphere itself. In stars, nuclear burning contributes to ϵ. In a protoplanetary atmosphere, dissipative drag on planetesimals contributes to ϵ. Our simplified models set $\epsilon = 0$, consistent with our neglect of planetesimal accretion luminosity at the base of the atmosphere. The $\epsilon_{\rm g} = -T\partial S/\partial t$ term gives the energy input from gravitational contraction.[1] The partial time derivative would normally require our radial derivatives to be partial derivatives. However, our subsequent developments will replace the local energy equation (10d) with global energy balance (see section §2.4), reverting the structure equations to time-independent ordinary differential equations (ODEs).

To solve the equation set (10) an equation of state (EOS) is required for closure. In our study, we adopt an ideal gas law with a polytropic EOS

$$P = \rho \mathcal{R} T \,, \qquad (13a)$$
$$P = K\rho^\gamma \,, \qquad (13b)$$

where K is the adiabatic constant. The adiabatic index $\gamma = 1/(1-\nabla_{\rm ad})$. An ideal monatomic gas has $\nabla_{\rm ad} = 2/5$. This work uses $\nabla_{\rm ad} = 2/7$ for an ideal diatomic gas. While our reference mean molecular weight ($\mu = 2.35$ proton masses) includes Helium, we ignore Helium's effect on the EOS, which is already greatly simplified. The second law or thermodynamics gives the relative entropy as

$$S = \mathcal{R}\ln\left(\frac{T^{1/\nabla_{\rm ad}}}{P}\right) \qquad (14)$$

eliminating the need for K.

Boundary conditions must be satisfied at both the base and the top of the atmosphere with $m(R_{\rm c}) = M_{\rm c}$, $T(R_{\rm H}) = T_{\rm d}$ and $P(R_{\rm H}) = P_{\rm d}$. In principle our solutions describe atmospheres with $L(R_{\rm c}) = 0$. In practice, since we do not directly integrate Equation (10d) we need not directly impose this boundary condition, as described in §2.5.

2.4. Global Cooling of an Embedded Planet

This section describes the global energy balance of a planet embedded in a gas disk, or more generally any spherical, hydrostatic object in pressure equilibrium with a background medium. The total atmospheric energy includes gravitational and internal energies, $E = E_G + U$:

$$E_G = -\int_{M_{\rm c}}^M \frac{Gm}{r}dm \,, \qquad (15a)$$

$$U = \int_{M_{\rm c}}^M u\,dm \,. \qquad (15b)$$

[1] In general, any motion in a non-stationary atmosphere is accounted for by this term. The partial time derivative is performed on shells of fixed mass.

The specific internal energy $u = C_V T = \mathcal{R}(\nabla_{\mathrm{ad}}^{-1} - 1)T$ for a polytropic EOS. For a star or coreless planet, $L_c = M_c = 0$.

We start with the global energy balance for an isolated planet of mass M with a free surface:

$$L_M = L_c + \Gamma - \dot{E}. \qquad (16)$$

The surface luminosity, L_M, includes contributions from the core luminosity L_c – e.g. planetesimal accretion or radioactive decay – from the total heat generation Γ – given by the integral of ϵ over the object – and from the rate of change of atmospheric energy $\dot{E}$, a loss term.

For an object with no core luminosity (or no core) and no internal heat sources, the energy equation $L_M = -\dot{E}$ describes KH contraction in its simplest form. For a main sequence star $L_M = \Gamma$ as the heat of nuclear burning supplies the total luminosity.

For a protoplanetary atmosphere embedded in a gas disk, the full energy equation,

$$L_M = L_c + \Gamma - \dot{E} + e_M \dot{M} - P_M \left. \frac{\partial V_M}{\partial t} \right|_M , \qquad (17)$$

acquires surface terms as derived in Appendix A. The energy accreted across the surface is given by the specific energy, $e_M = u_M - GM/R$, and the mass accretion rate of gas, $\dot{M}$. The work done by the surface is $P_M \partial V_M / \partial t$, with the partial derivative performed at fixed mass. This generalized energy equation applies on any spherical shell where hydrostatic balance holds.[2] Thus M no longer refers to a uniquely defined total mass, but to the chosen mass level, where the instantaneous radius is R. Values on this shell are labelled by M subscripts.

For static solutions, which are not the focus of this Paper, the surface terms (and also $\dot{E}$) vanish. Static solutions are valid when imposed heat sources, i.e. L_c and Γ exceed the atmospheric losses. Quantitatively, static solutions apply when the evolutionary timescale exceeds the KH timescale,

$$\tau_{\mathrm{KH}} \sim \frac{|E|}{L_M}, \qquad (18)$$

where surface terms are assumed to be subdominant. Thus evolutionary calculations, including the quasistatic calculations of this Paper, are needed to consider the fastest possible evolution that occurs on τ_{KH}.

2.5. *The Two-Layer Model*

To simplify our calculations of atmospheric contraction we use a two layer model with a bottom convective region and an upper radiative layer. The existence of such a structure is well known from previous studies (e.g., R06) and can be readily understood. Before the protoplanetary atmosphere can cool, it has the entropy of the disk. As the atmosphere cools the deep interior remains convective. Convective interiors are a common feature of low mass cool objects (brown dwarfs and planets) that

results from the behavior of ∇_{rad} for realistic opacity laws. However the entropy of the deep interior decreases as the atmosphere cools. A region of outwardly increasing entropy, i.e. a radiative layer, is required to connect the convective interior to the disk. A more complicated structure, with radiative windows in the convection zone, is possible as discussed in §**??**.

In convective regions, the adiabatic structure is independent of luminosity and can be calculated without local energy balance, Equation (10d). Thus for fully convective objects, a cooling sequence can be established by connecting a series of adiabatic solutions using a global energy equation, $L_M = -\dot{E}$ or Equation (16). Such methods are commonly used for their computational efficiency and are sometime referred to as "following the adiabats," since the steady state solutions evolve in order of decreasing entropy (Marleau & Cumming 2013).

In the radiative zone, local energy balance, Equation (10d), does affect the atmospheric structure. We proceed by assuming that the majority of energy is lost from the convective interior, and thus the luminosity can be treated as constant in the outer radiative zone. With this approximation we can construct solutions from equations (10a – c) that "follow the mass," i.e. gradually increase the atmospheric mass. We then use the global energy balance, Equation (17) to connect these solution in a cooling sequence. The validity of neglecting luminosity generation in the radiative zone can be checked *a posteriori*.

To make a single atmosphere model (indexed by i) we choose a planet mass M_i. At the outer boundary, at $R_{\mathrm{H}}(M_i)$, the temperature and pressure are set to the disk values. To integrate equations (10a–c), the luminosity is required to compute ∇_{rad}. The correct value of the luminosity is the eigenvalue of the problem, which we find by the shooting method (Press et al. 2002). Only for the eigenvalue of luminosity does the integrated value of mass at the core, $m(R_c)$, match the actual core mass, M_c.

To establish the time difference between neighboring solutions, we apply Equation (17) at the radiative-convective boundary (RCB) of the solutions. Using exact solutions, energy balance could be evaluated at any level. The approximation of constant luminosity in the radiative zone makes the RCB the self-consistent choice. After setting $\Gamma = L_c = 0$, we solve for the elapsed time Δt between states i and $i+1$ by finite differencing to give

$$\Delta t = \frac{-\Delta E + \langle e \rangle \Delta M - \langle P \rangle \Delta V_{\langle M \rangle}}{\langle L \rangle}. \qquad (19)$$

Brackets indicate an average of, and Delta (Δ) indicates a difference between, neighboring solutions. All values are evaluated at the RCB. Due to the partial derivative in Equation (17), the volume difference $\Delta V_{<M>}$ is performed at fixed mass, here the average of the masses at the RCB.

3. ANALYTIC COOLING MODEL

This section develops the analytic version of our two-layer model, which is useful for predicting and explaining the results of numerical evolution models. To obtain our analytic results, we neglect self-gravity. As shown in Section 4, self-gravity becomes quantitatively important

---

[2] Equation (17) also applies in the interior of objects with a free surface. The work term, $P_M \partial V_M / \partial t$, vanishes at the free surface. The accretion energy, $e_M \dot{M}$, vanishes for a truly isolated object, but would be included to account for accretion onto (or mass loss from) an otherwise free surface.

at surprisingly low atmospheric masses, $M_{\rm atm} \gtrsim 0.2 M_{\rm c}$. Thus the analytic model cannot accurately model the the later stages of evolution. Nevertheless, the analytic model does successfully explain general trends with opacity and disk temperature and pressure, for example.

The analytic model also assumes that the upper radiative radiative layer is thick, with a pressure depth $P_{\rm RCB} \gg P_{\rm d}$. This approximation limits the ability to study the initial cooling of very low mass atmospheres with thin outer radiative zones. However since early evolution is quite rapid, this approximation negligibly affects total cooling times and critical core masses, our main foci.

3.1. *Two Layer Structure*

To apply the two layer cooling model analytically, we require expressions for the atmospheric structure. Conditions at the RCB are crucial as they set the interior adiabat and the radiative losses. (Recall that luminosity generation in the radiative zone is neglected.) We express the temperature and pressure of the RCB, at the radius $R_{\rm RCB}$, as

$$T_{\rm RCB} = \chi T_{\rm d} \tag{20a}$$
$$P_{\rm RCB} = \theta P_{\rm d} e^{R_{\rm B}/R_{\rm RCB}} . \tag{20b}$$

If the radiative zone were replaced by an isothermal layer, then hydrostatic balance would give $\chi = \theta = 1$. Standard radiative structure calculations (see Appendix B for details) give

$$\chi \simeq \left(1 - \frac{\nabla_{\rm ad}}{\nabla_\infty}\right)^{-\frac{1}{4-\beta}} \simeq 1.53 \,, \tag{21}$$

for $P_{\rm RCB} \gg P_{\rm d}$, our regime of interest, and with the radiative temperature gradient at infinite depth, $\nabla_\infty = 1/2$, for our dust opacity. The radiative zones are thus nearly isothermal, as also found by R06. While a simple closed form expression is not possible, the factor $\theta \simeq 0.556$ for our parameters. According to Equation (20b) our pressure criterion also gives $R_{\rm RCB} \ll R_{\rm B}$, but the inequality is logarithmically weaker.

Given the conditions at the RCB, hydrostatic balance gives the density and temperature profiles in the inner region along the adiabat,

$$\rho = \rho_{\rm RCB} \left[1 + \frac{R_{\rm B}'}{r} - \frac{R_{\rm B}'}{R_{\rm RCB}}\right]^{1/(\gamma-1)} \tag{22a}$$

$$T = T_{\rm RCB} \left[1 + \frac{R_{\rm B}'}{r} - \frac{R_{\rm B}'}{R_{\rm RCB}}\right] . \tag{22b}$$

The effective Bondi radius

$$R_{\rm B}' \equiv \frac{GM_{\rm c}}{C_P T_{\rm RCB}} = \frac{\nabla_{\rm ad}}{\chi} R_{\rm B} \tag{23}$$

simplifies expressions, with $C_P = \mathcal{R}/\nabla_{\rm ad}$ the specific heat at constant pressure.

Even simpler expressions hold deep in the adiabatic interior, where $r \ll R_{\rm RCB} \ll R_{\rm B}'$ gives

$$\rho \simeq \rho_{\rm RCB} \left[\frac{R_{\rm B}'}{r}\right]^{1/(\gamma-1)} \propto r^{-5/2} \tag{24a}$$

$$T \simeq T_{\rm RCB} \frac{R_{\rm B}'}{r} = \frac{GM_{\rm c}}{C_P r} . \tag{24b}$$

While the radial density profile depends on the adiabatic index, the temperature scaling does not. For reference, if self-gravity is included, the temperature profile satifies

$$\frac{dT}{dr} = -\frac{Gm(r)}{C_P r^2} . \tag{25}$$

Thus the enclosed mass in self-gravitating models gives a temperature profile flatter than $T \propto r^{-1}$.

The total specific energy at depth

$$e = e_g + u = -\nabla_{\rm ad} \frac{GM_{\rm c}}{r} . \tag{26}$$

is thus generically proportional to the gravitational potential, $e_g = -GM_{\rm c}/r$.

3.2. *Mass, Energy and Luminosity*

The most relevant quantities for the global cooling model (equation 17) are the integrated energy, luminosity, and atmospheric mass. In our non-self-gravitating limit, the mass of our nearly isothermal radiative zones is less than the convective interior, as shown in Appendix B.

Equation (22a) thus integrates to give the atmospheric mass

$$M_{\rm atm} = \frac{5\pi^2}{4} \rho_{\rm RCB} R_{\rm B}'^{5/2} \sqrt{R_{\rm RCB}}, \tag{27}$$

in the relevant limit $R_{\rm c} \ll R_{\rm RCB} \ll R_{\rm B}'$ and for $\gamma = 7/5$. Mass is concentrated near the outer regions of the convective zone, a result that holds more generally for $\gamma > 4/3$.

Using Equation (20b) to eliminate $R_{\rm RCB}$, the critical ratio of atmosphere to core mass becomes

$$\frac{M_{\rm atm}}{M_{\rm c}} = \frac{P_{\rm RCB}}{\xi P_M}, \tag{28}$$

where we define a characteristic pressure and a logarithmic factor

$$P_M \equiv \frac{4\nabla_{\rm ad}^{3/2}}{5\pi^2 \sqrt{\chi}} \frac{GM_{\rm c}^2}{R_{\rm B}'^4} \tag{29a}$$

$$\xi \equiv \sqrt{\ln[P_{\rm RCB}/(\theta P_{\rm d})]} . \tag{29b}$$

The atmosphere mass increases as radiative losses lower the internal adiabat and increase $P_{\rm RCB}$. The crossover mass, $M_{\rm atm} = M_{\rm c}$, is reached when

$$P_{\rm RCB} = \xi P_M, \tag{30}$$

i.e. near the characteristic pressure P_M. The critical value of the order unity factor ξ is found by eliminating $P_{\rm RCB}$ from Equations (29b) and (30). This logarithmic factor complicates our analytic description, but since it remains order unity we simply hold it fixed in our scalings.

The total energy is concentrated towards the core if $u\rho r^3 \propto \rho r^2$ drops with increasing r. This condition requires $\gamma < 3/2$, which our choice of $\gamma = 7/5$ satisfies, but $\gamma = 5/3$ does not. Integration of Equation (26) over the

mass of the atmosphere thus gives

$$E = -4\pi\nabla_{\mathrm{ad}}GM_{\mathrm{c}}\int_{R_{\mathrm{c}}}^{R_{\mathrm{RCB}}}\rho r\,dr \qquad (31\mathrm{a})$$

$$\approx -4\pi P_{\mathrm{RCB}}R_{\mathrm{B}}'^{\frac{1}{\nabla_{\mathrm{ad}}}}\left(\frac{\gamma-1}{3-2\gamma}\right)R_{\mathrm{c}}^{\frac{2\gamma-3}{\gamma-1}} \qquad (31\mathrm{b})$$

$$\approx -8\pi P_{\mathrm{RCB}}\frac{R_{\mathrm{B}}'^{7/2}}{\sqrt{R_{\mathrm{c}}}} \qquad (31\mathrm{c})$$

with $\gamma < 3/2$ and $\gamma = 7/5$ in Equations (31b) and (31c), respectively.

Applying marginal convective stability, $\nabla_{\mathrm{rad}} = \nabla_{\mathrm{ad}}$, to Equation (11) gives the emergent luminosity from the radiative-convective boundary,

$$L_{\mathrm{RCB}} = \frac{64\pi GM_{\mathrm{RCB}}\sigma T_{\mathrm{RCB}}^4}{3\kappa P_{\mathrm{RCB}}}\nabla_{\mathrm{ad}} \approx L_{\mathrm{d}}\frac{P_{\mathrm{d}}}{P_{\mathrm{RCB}}}, \qquad (32)$$

where we define

$$L_{\mathrm{d}} \equiv \frac{64\pi GM_{\mathrm{RCB}}\sigma T_{\mathrm{d}}^4}{3\kappa(T_{\mathrm{d}})P_{\mathrm{d}}}\nabla_{\mathrm{ad}}\chi^{4-\beta}. \qquad (33)$$

The inverse scaling $L_{\mathrm{RCB}} \propto 1/P_{\mathrm{RCB}}$ shows that luminosity drops as the atmosphere cools and P_{RCB} deepens. This result relies on the pressure independence of dust opacities. For fully non-self-gravitating results, we replace M_{RCB}, the mass up to the RCB, with the core mass, but the mass of the convective atmosphere could be included for a slightly higher order estimate.

3.3. Simplified Cooling Model

Our analytic cooling model uses $L = -\dot{E}$, neglecting the surface terms in Equation (17).[3] Applying Equations (31c) and (32), the time it takes to cool the atmosphere until the RCB reaches a given pressure depth, P_{RCB}, is

$$t_{\mathrm{cool}} = -\int_{P_{\mathrm{d}}}^{P_{\mathrm{RCB}}}\frac{dE/dP_{\mathrm{RCB}}}{L_{\mathrm{RCB}}}dP_{\mathrm{RCB}} \qquad (34\mathrm{a})$$

$$\approx 4\pi\frac{P_{\mathrm{RCB}}^2}{P_{\mathrm{d}}}\frac{R_{\mathrm{B}}'^{7/2}}{L_{\mathrm{d}}\sqrt{R_{\mathrm{c}}}}. \qquad (34\mathrm{b})$$

The initial RCB depth, set to P_{d} as a formality, is of little importance because the cooling slows as it proceeds with $t_{\mathrm{cool}} \propto P_{\mathrm{RCB}}^2$.

The most relevant cooling time is the crossover time, t_{co}, required to reach the crossover mass, $M_{\mathrm{atm}} = M_{\mathrm{c}}$. Equations (34) and (30) give this time as

$$t_{\mathrm{co}} \approx 2\times 10^8\frac{F_T^{5/2}F_\kappa\left(\frac{\xi}{3.4}\right)^2}{m_{\mathrm{c}10}^{5/3}a_{10}^{15/14}}\,\mathrm{yr}. \qquad (35)$$

The corresponding critical core mass, M_{crit}, has a crossover time that equals the typical lifetime of a protoplanetary disk

$$t_{\mathrm{d}} = 3\times 10^6\,\mathrm{yr}. \qquad (36)$$

---

[3] Appendix B shows that these terms are negligible for a non-self-gravitating model, but they do become relevant when self-gravity is important and included.

Setting $t_{\mathrm{co}} = t_{\mathrm{d}}$ gives

$$M_{\mathrm{crit}} \approx 100\frac{F_T^{3/2}F_\kappa^{3/5}\left(\frac{\xi}{2.6}\right)^{6/5}}{a_{10}^{9/14}}\,M_\oplus. \qquad (37)$$

Both t_{co} and M_{crit} are too large to be interesting, or to be correct based on previous results and the numerical results in this Paper. The main reason for this discrepancy is the neglect of self-gravity, as shown in Section 4. The magnitude of the discrepancy may be surprising as one might expect self-gravity to be a modest factor for $M_{\mathrm{atm}} \leq M_{\mathrm{c}}$. Clearly this seemingly reasonable expectation must be applied with caution, an interesting result in itself.

The analytic model is also useful because, despite the amplitude error, it explains the basic scaling of our (and other) numerical models. As is well known, a lower opacity, here scaling with F_κ, accelerates growth and gives a lower critical core mass. Lower disk temperatures also decrease both t_{co} and M_{crit}. Furthermore the decline in both quantities with semimajor axis is completely generated by the disk temperature law (ignoring ξ). The temperature dependence are a competition between two main effects. The higher luminosity, $\propto T^{4-\beta}$, at higher temperatures gives faster cooling, which opposes the overall effect. The larger Bondi radius, and the effectively stronger gravity of the core, is the dominant effect that gives faster cooling at lower temperatures. For different β values, $t_{\mathrm{co}} \propto F_T^{\beta+1/2}$, so the slope of the dust opacity is an important moderating effect on the cooling.

The cooling timescale and critical core mass depend only weakly on the disk pressure, via the logarithmic factor ξ. Section 5.1 shows that these analytic predictions for disk temperature and pressure dependence compare favorably with numerical results.

TODO: consider adding "revised" analytic expressions for t_{co} and M_{crit} (e.g. lower Matm criterion). People like scalings, but the obviously wrong amplitudes will prevent people from using them unless we correct.

4. QUASI-STATIC KELVIN-HELMHOLTZ CONTRACTION

We now present some representative examples of the structure and evolution of our model atmospheres, calculated as described in §2, with some comparisons made to the non-self-gravitating analytic model of §3. Radial structure is presented in §4.1, time evolution is described in §4.2 and the regimes of validity of our two-layer cooling model are examined in §4.3.

4.1. Atmospheric Stucture

Figure 1 shows radial profiles at different stages of atmospheric growth. In these examples, we fix the core mass at $M_{\mathrm{c}} = 5M_\oplus$ and the radial disk location to $a = 60$ AU. The quoted mass values include the core plus atmosphere within the smaller of R_{B} or R_{H}, which for these cases is R_{B}. The 9.24 $M_\oplus$ solution is the highest mass we can reach in our evolutionary sequence, as we explain further in §4.3.

Deep in a non-self-gravitating atmosphere, Equation (24) shows that $T \propto r^{-1}$ and $P \propto r^{-1/\nabla_{\mathrm{ad}}}$. This behavior is seen in the low mass solutions in Fig. 1. As
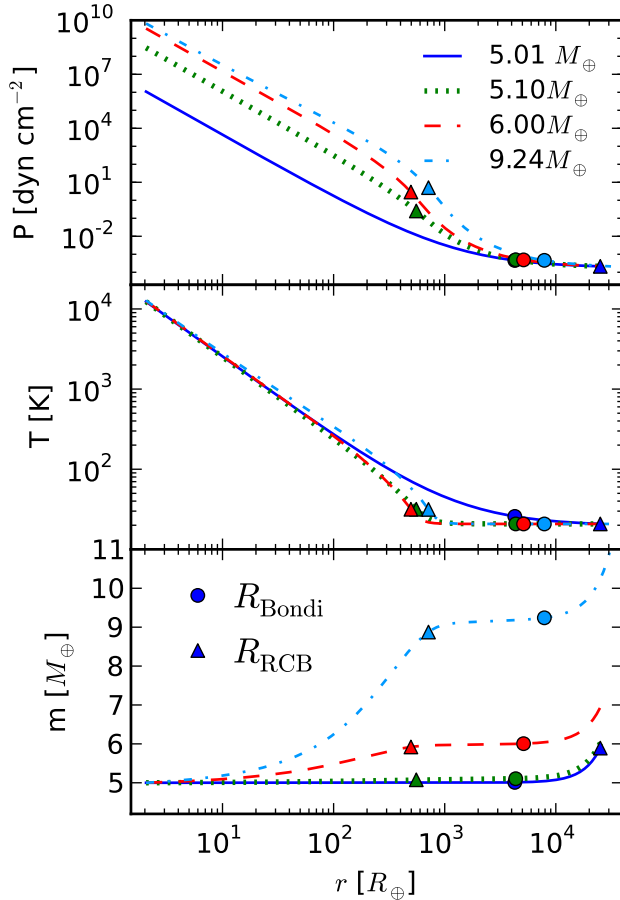
FIG. 1.— Radial profiles of atmospheric pressure, temperature and enclosed mass (including the core) for a $5M_\oplus$ core at $a = 60$ AU. Solid, dotted and dashed lines correspond to solutions with total mass (core and atmosphere) of $5.01M_\oplus$, $5.10M_\oplus$, $6.00M_\oplus$ and $9.24M_\oplus$, respectively. (See text for a description of evolution to yet higher masses.) Circles and triangles mark the locations of the Bondi radii and of the radiative-convective boundaries, respectively. The radial profiles extend from the core to the Hill radius.

explained by Equation (25), the higher mass solutions show a flatter profile in T and also in $P \propto T^{1/\nabla_{\rm ad}}$. In agreement with Equation (20), the radiative zone remains nearly isothermal – even in the more massive solutions – and thus shows a nearly exponential increase in pressure with inverse depth.

The atmosphere starts out as purely convective and isentropic, as seen in Fig. 1 for the 5.01 $M_\oplus$ solution which has no radiative zone. Further gas accumulation brings in energy that has to be radiated away, forming a radiative region that quickly deepens. The fast pressure deepening of the radiative region is evident in Fig. 1 — even a low mass atmosphere (i.e. the 5.10 $M_\oplus$ solution) has an extended radiative zone.

The higher mass atmosphere solutions have lower entropy, i.e. cooling allows the atmosphere to accrete more gas. This is evident in Fig. 1 from the higher internal pressures of the higher mass solutions. The somewhat higher temperatures in the higher mass solutions do not cause the entropy to increase.
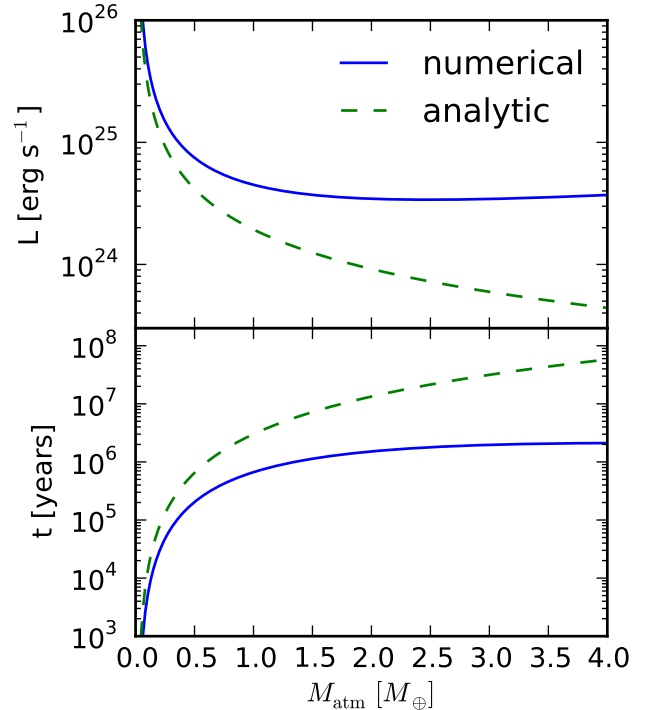

FIG. 2.— Evolution of the luminosity and elapsed time during atmospheric growth around a $5M_\oplus$ core at 60 AU. The luminosity is initially high, then decreases as the atmosphere grows in mass and the radiative zone becomes optically thicker. Due to the neglect of self-gravity, the analytic model (*dashed curve*) gives a further drop in luminosity and a longer evolution time.

4.2. Time Evolution

The cooling model of §2.5 is used to connect solutions of different atmospheric masses into an evolutionary sequence. Fig. 2 shows the luminosity evolution and the elapsed time as a function of atmospheric mass for a $5M_\oplus$ core at 60 AU, i.e. the same parameters as in Fig. 1. During the early stages of atmospheric growth, the luminosity drops sharply. This behavior is seen in both the full numerical solutions (with solid lines) and the analytic model (with dashed lines). As seen in Equation (32), the increased pressure depth of the RCB increases the optical depth ($\propto \kappa P$) and decreases the radiative luminosity.

At later stages of evolution, the numerical model gives a flat luminosity with increasing mass and also time (not shown). By contrast the analytic model gives a luminosity that continues to drop with increasing mass. The difference is due to the neglect of self-gravity in the analytic model. From Equation (32), $L_{\rm RCB} \propto M_{\rm RCB} T_{\rm RCB}^4/(\kappa_{\rm RCB} P_{\rm RCB})$. Thus accounting for the higher enclosed mass gives a somewhat higher luminosity in the self-gravitating model. However, the main effect is the higher temperature in the self-gravitating models. The flatter temperature profiles with radius, as described above, explain why the self-gravitating models are hotter.

Before discussing time evolution (both the elapsed time from the bottom panel of Fig. 2 and the characteristic growth time of the atmosphere), we briefly discuss the effect of decreasing the atmospheric dust abundance on
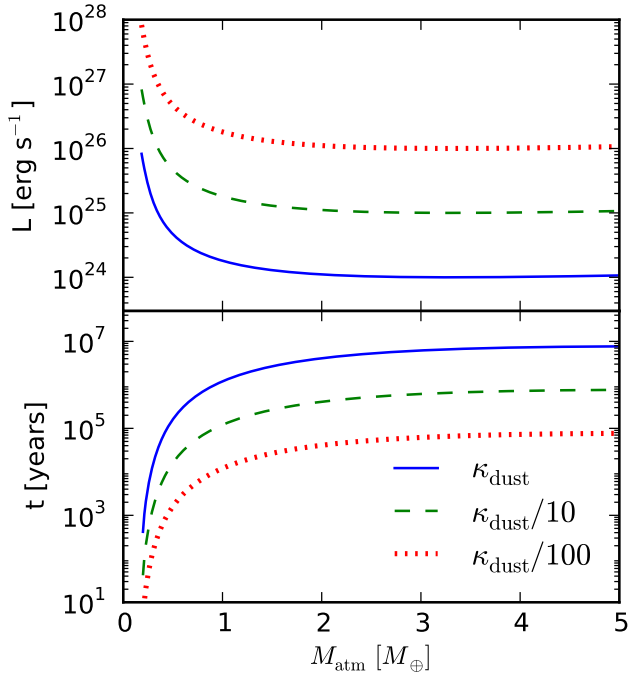
FIG. 3.— Similar to Fig. 2, but showing the effect of reducing the dust abundance by factors of 10 and 100 from standard Solar abundances. The reduced dust opacities give higher luminosities and faster atmospheric growth.

the atmospheric evolution. In Fig. 3, the opacity normalization in Equation (5) is reduced by factors of 10 and 100. Lower opacities result in higher luminosities and faster evolution, a well-established result (Hubickyj et al. 2005) that we confirm for our model. Atmospheric dust opacities are difficult to robustly predict. Ablation of infalling solids is a dust source, while settling through the radiative zone is a sink. Grain growth both reduces dust opacities per unit mass and favors settling. Our scenario of negligible ongoing particle accretion tends to favor low dust opacities. To be conservative, however, our reference case considers full Solar abundances, but faster evolution is clearly possible. The effect of opacity reduction on the critical core mass is deferred to §5.

Fig. 4 plots the evolution of the atmospheric growth timescale, $M_{\rm atm}/\dot{M}$, around a $5M_\oplus$ core at several locations in the disk. This instantaneous growth time shows clearly that the atmosphere spends the bulk of its time growing though intermediate atmospheric masses, $\sim 1-3$ $M_\oplus$ in this case. Growth times are short both early – when the radiative zone is relatively transparent – and late – when self-gravity accelerates growth. The accelerated growth at higher masses is also evident in Figs. 2 and 3 (bottom panels) as the flattening of the t vs. $M_{\rm atm}$ curve.

The fact that growth times peak before the crossover mass, when $M_{\rm atm} < M_{\rm c}$, is very helpful for understanding atmospheric growth. The estimated timescale to runaway growth can be well approximated by only considering the time it takes to grow to the crossover mass, or even to a somewhat lower mass. This insensitivity to the upper mass threshold is characteristic of accelerating
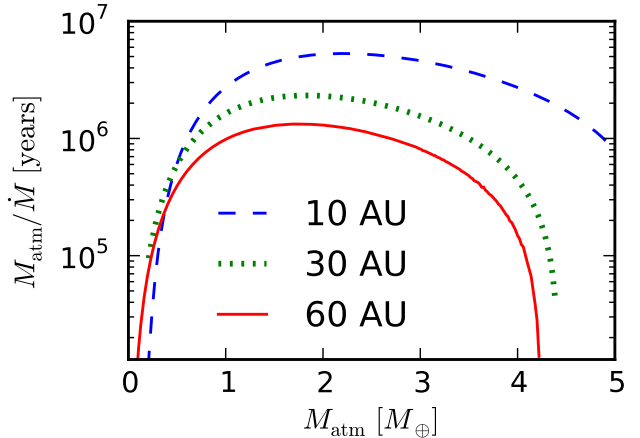

FIG. 4.— Evolution of the atmospheric growth timescale with mass around a $5M_\oplus$ solid core located at 10, 30 or 60 AU. Growth is slowest for $M_{\rm atm} \sim 1-3M_\oplus$, i.e. before the crossover mass at $M_{\rm atm} = M_{\rm c}$.

growth, and is fortuitous. We next show how our model assumptions can break down during the later stages of atmospheric growth.

### 4.3. Validity of the Two-Layer Cooling Model

To examine the regimes where our cooling model is valid, we compare the model luminosity to the additional neglected luminosity, $L_{\rm negl}$, that a more detailed model would have generated in the radiative zone. To compute $L_{\rm negl}$ we compute the entropy difference between successive radiative zone solutions. We then integrate the energy equation, $\partial L/\partial m = -T\partial S/\partial t$, over the average depth of the radiative zone.[4]

Fig. 4.3 shows that the neglected luminosity is indeed negligible during the early stages of evolution. However, $L_{\rm negl}$ exceeds the model luminosity, L, at high masses, $M_{\rm atm} > 3M_\oplus$ in this case, meaning that our model is becoming inaccurate. Nevertheless, our cooling model gives both conservative and reasonably reliable estimates of core accretion timescales. Our results are conservative – in the sense of overestimating growth times – because the neglected luminosity would give more rapid evolution. Moreover, our results are reasonably accurate because the bulk of growth time is spent at low masses, when $L_{\rm negl}$ is small and safely neglected.

The (non-vanishing) individual terms in the global cooling model of Equation (17), evaluated at the RCB, are also plotted in Fig. 4.3. At low masses, the change in energy, $-\dot{E}$, makes the dominant contribution to luminosity. As the mass increases the surface terms become more significant, led by the accretion energy. However the surface terms are everywhere smaller than $L_{\rm negl}$. Thus while the surface terms appear to reduce the total luminosity (compared to $-\dot{E}$), $L_{\rm negl}$ can more than compensate, showing again that our model conservatively underestimates cooling.

At yet higher masses than shown in Fig. 4.3, our cool-

---

[4] While useful as a diagnostic, the neglected luminosity cannot reliably correct the global cooling model because where $L_{\rm negl}$ is significant, the structure of the radiative zone would be inaccurate.
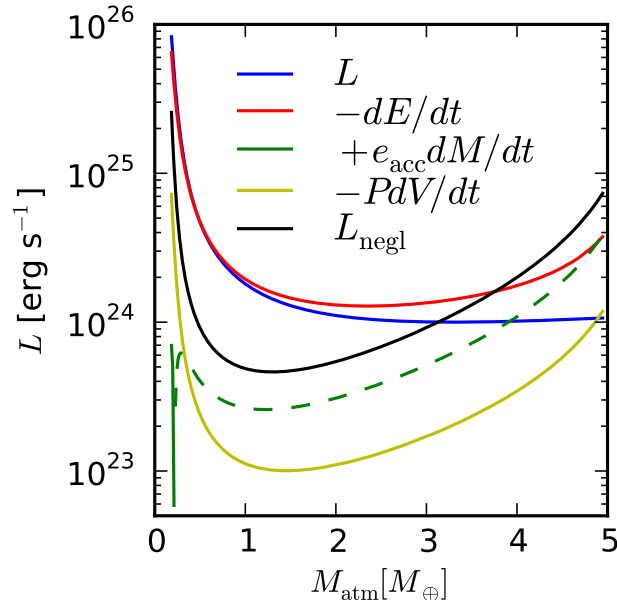
ing model breaks down. Mathematically, the break-down manifests as negative timesteps when advancing to a higher atmospheric mass. This unphysical result has no deep significance, as we already know that the neglected luminosity is large enough to give incorrect results. Sometimes this breakdown occurs even before the crossover mass is reached. The main practical effect of this behavior is that we halt the evolution where the model breaks down whenever we cannot reach the crossover mass. Fortunately, the elapsed time to either the crossover mass or the breakdown is well-behaved and, most importantly, dominated by lower atmospheric masses where the model is accurate.

5. CRITICAL CORE MASS

5.1. *Disk Temperature and Pressure*

6. NEGLECTED EFFECTS

6.1. *Hydrodynamic Effects*

The neglect of hydrodynamical effects in our model is best discussed in terms of the thermal mass, $M_{\rm th}$, and the length scales introduced in §2.2. In the low mass regime, $M_{\rm p} < M_{\rm th}/\sqrt{3}$, where $R_{\rm B} < R_{\rm H}$, we assume that hydrostatic balance holds out to the outer boundary at $R_{\rm H}$. In this low mass regime, Ormel (2013) calculated the flow patterns driven by stellar tides and disk head-winds. On scales $\gtrsim R_{\rm B}$ the flows no longer circulate the planet: they belong to the disk. Nevertheless, the density

structure outside $R_{\rm B}$ remains spherically symmetric and hydrostatic. Even if these flows do not destroy hydro-static balance, they could affect the planet's cooling. We expect such effects to be weak, as heat losses at greater depths dominate planetary cooling, but more study is needed.

At higher masses, non-hydrostatic effects become more severe. At $M_{\rm p} \gtrsim M_{\rm th}$ planets can open significant gaps (Zhu et al. 2013). At yet higher masses accretion insta-bilities could occur (Ayliffe & Bate 2012). However, in this high mass regime we already know that the spheri-cally symmetric approximation breaks down (see §2.2).

Thus by restricting our attention to low masses, ne-glected hydrodynamic effects should be minor. More-over since $M_{\rm th} \propto a^{6/7}$ increases with disk radius, spheri-cal hydrostatic models like ours have a greater range of applicability in the outer regions of disks.

6.2. *Realistic Opacities*

Real dust opacities exhibit a more complicated behav-ior that depends on grain composition. Opacities drop by order unity when ice grains sublimate for $T \gtrsim 150$ K and they drop by orders of magnitude when silicate grains evaporate above $T \gtrsim 1500$ K (Semenov et al. 2003; Fer-guson et al. 2005). Our model assumes that radiative regions only exist in the outer part of the atmosphere. As such, even though protoplanetary atmospheres get significantly hotter than 1500 K, our model depends on opacity only in the upper radiative zones, which are cool enough to remain dusty. For our opacity approximations to be valid, we must restrict our model to the lower tem-peratures of the outer disk.

A second radiative zone inside the convection zone, a "radiative window," is possible, due to the opacity drops caused by the evaporation of ice and metal grains. Our two layer model ignores such complications. Grain growth also impacts the opacity in the outer regions as well as the existence or depth of radiative windows. We explore more realistic opacity laws in In Piso et al. (2013, in prep.).

6.3. *Equation of State*

In our model we assume an ideal gas law and a poly-tropic EOS, given by equations (13a) and (13b), respec-tively. However, non-ideal effects such as partial dissoci-ation and ionization have to be taken into account. One solution is using tabulated equation of state tables for hydrogen and helium mixtures. In Piso et al. (2013, in prep) we use the Saumon et al. (1995) EOS tables and extend them to lower pressures and temperatures as re-quired by our disk assumptions.

7. CONCLUSIONS

REFERENCES

Alibert, Y., Mordasini, C., Benz, W., & Winisdoerffer, C. 2005, A&A, 434, 343
Arras, P. & Bildsten, L. 2006, ApJ, 650, 394
Ayliffe, B. A. & Bate, M. R. 2012, MNRAS, 427, 2597
Bell, K. R. & Lin, D. N. C. 1994, ApJ, 427, 987
Bodenheimer, P. & Pollack, J. B. 1986, , 67, 391
Boss, A. P. 1997, Science, 276, 1836
Chiang, E. & Youdin, A. N. 2010, Annual Review of Earth and Planetary Sciences, 38, 493

D'Angelo, G., Durisen, R. H., & Lissauer, J. J. Giant Planet Formation, ed. S. Piper, 319–346
Dones, L. & Tremaine, S. 1993, , 103, 67
Ferguson, J. W., Alexander, D. R., Allard, F., Barman, T., Bodnarik, J. G., Hauschildt, P. H., Heffner-Wong, A., & Tamanai, A. 2005, ApJ, 623, 585
Fortney, J. J., Marley, M. S., & Barnes, J. W. 2007, ApJ, 659, 1661

Harris, A. W. 1978, in Lunar and Planetary Institute Science Conference Abstracts, Vol. 9, Lunar and Planetary Institute Science Conference Abstracts, 459–461

Hubickyj, O., Bodenheimer, P., & Lissauer, J. J. 2005, , 179, 415

Ikoma, M., Nakazawa, K., & Emori, H. 2000, ApJ, 537, 1013

Kenyon, S. J. & Bromley, B. C. 2009, ApJ, 690, L140

Kippenhahn, R. & Weigert, A. 1990, Stellar Structure and Evolution

Kratter, K. M., Murray-Clay, R. A., & Youdin, A. N. 2010, ApJ, 710, 1375

Lambrechts, M. & Johansen, A. 2012, A&A, 544, A32

Marleau, G.-D. & Cumming, A. 2013, arXiv:1302.1517

Menou, K. & Goodman, J. 2004, ApJ, 606, 520

Mizuno, H., Nakazawa, K., & Hayashi, C. 1978, Progress of Theoretical Physics, 60, 699

Ormel, C. W. 2013, MNRAS, 428, 3526

Papaloizou, J. C. B. & Nelson, R. P. 2005, A&A, 433, 247

Pollack, J. B., Hubickyj, O., Bodenheimer, P., Lissauer, J. J., Podolak, M., & Greenzweig, Y. 1996, , 124, 62

Press, W. H., Teukolsky, S. A., Vetterling, W. T., & Flannery, B. P. 2002, Numerical recipes in C++ : the art of scientific computing

Rafikov, R. R. 2005, ApJ, 621, L69

—. 2006, ApJ, 648, 666

Saumon, D., Chabrier, G., & van Horn, H. M. 1995, ApJS, 99, 713

Semenov, D., Henning, T., Helling, C., Ilgner, M., & Sedlmayr, E. 2003, A&A, 410, 611

Stevenson, D. J. 1982, Planet. Space Sci., 30, 755

Wuchterl, G. 1993, , 106, 323

Youdin, A. N. & Mitchell, J. L. 2010, ApJ, 721, 1113

Zhu, Z., Stone, J. M., & Rafikov, R. R. 2013, ApJ, 768, 143

APPENDIX

A. DERIVATION OF THE GLOBAL ENERGY EQUATION

To derive the global energy equation (17) for an embedded protoplanets, we generalize the analogous calculations in stellar structure theory, e.g. in §4.3 of Kippenhahn & Weigert (1990). For our problem we add the effects of finite core radius, surface pressure and mass accretion. We start with the local energy equation (10d) whose more natural form in Lagrangian (mass) coordinates is $\partial L/\partial m = \epsilon - T\partial S/\partial t$. Integrating from the core to a higher shell with enclosed mass M gives:

$$L - L_c = \int_{M_c}^{M} \frac{\partial L}{\partial m} dm \tag{A1a}$$

$$= \int_{M_c}^{M} \left(\epsilon - T\frac{\partial S}{\partial t}\right) dm \tag{A1b}$$

$$= \Gamma - \int_{M_c}^{M} \frac{\partial u}{\partial t} dm + \int_{M_c}^{M} \frac{P}{\rho^2}\frac{\partial \rho}{\partial t} dm . \tag{A1c}$$

with $\Gamma = \int \epsilon dm$ the integral of the direct heating rate and applying the law of thermodynamics in the final step.

The global energy equation is derived by eliminating the partial time derivatives in Equation (A1c), which are performed at a fixed mass, in favor of total time derivatives, denoted with overdots. For instance the surface radius, R, evolves as

$$\dot{R} = \frac{\partial R}{\partial t} + \frac{\dot{M}}{4\pi R^2 \rho_M} \tag{A2}$$

where $\partial R/\partial t$ gives the Lagrangian contraction of the "original" shell, and mass accretion through the upper boundary at rate $\dot{M}$ also changes the shell location. Similarly the volume, $V = (4\pi/3)r^3$, and pressure at the outer shell evolve as

$$\dot{V}_M = \frac{\partial V_M}{\partial t} + \frac{\dot{M}}{\rho_M} \tag{A3a}$$

$$\dot{P}_M = \frac{\partial P_M}{\partial t} + \frac{\partial P_M}{\partial m}\dot{M} = \frac{\partial P_M}{\partial t} - \frac{GM}{4\pi R^4}\dot{M} . \tag{A3b}$$

This derivation holds the core mass and radius fixed, $\dot{M}_c = \dot{R}_c = 0$. Therefore the core pressure satisfies

$$\dot{P}_c = \partial P_c/\partial t . \tag{A4}$$

The internal energy integral follows simply from Leibniz's rule as

$$\int_{M_c}^{M(t)} \frac{\partial u}{\partial t} dm = \dot{U} - \dot{M} u_M . \tag{A5}$$

To make further progress we require the virial theorem:

$$E_G = -3\int_{M_c}^{M} \frac{P}{\rho} dm + 4\pi(R^3 P_M - R_c^3 P_c) \tag{A6}$$

which follows from Equations (10a), (10b) and (15) by integrating hydrostatic balance in Lagrangian coordinates. As an aside, the integral in equation (A6) can be evaluated for a polytropic EOS to give simple expressions for the total

energy:

$$E = (1 - \zeta)U + 4\pi(R^3 P_M - R_c^3 P_c) \tag{A7a}$$

$$= \frac{\zeta - 1}{\zeta}E_G + \frac{4\pi}{\zeta}(R^3 P_M - R_c^3 P_c) \tag{A7b}$$

where $\zeta \equiv 3(\gamma - 1)$. We will not make this assumption and will keep the EOS general.

To express the work integral, the final term in Equation (A1c), in terms of changes to gravitational energy we first take the time derivative of Equation (A6):

$$\dot{E}_G = 3 \int_{M_c}^{M} \frac{P}{\rho^2}\frac{\partial \rho}{\partial t}dm - 3 \int_{M_c}^{M} \frac{\partial P}{\partial t}\frac{dm}{\rho} - 3\frac{P_M}{\rho_M}\dot{M} + 3\dot{P}_M V_M - 3\dot{P}_c V_c + 3P_M \dot{V}_M . \tag{A8}$$

The first integral in Equation (A8) is the one we want, but the next one must be eliminated. The time derivative of Equation (15) (times four) gives

$$4\dot{E}_G = -4\frac{GM\dot{M}}{R} + 4\int_{M_c}^{M}\frac{Gm}{r^2}\frac{\partial r}{\partial t}dm \tag{A9a}$$

$$= -4\frac{GM\dot{M}}{R} + 4\pi\int_{M_c}^{M} r^3\frac{\partial}{\partial m}\frac{\partial P}{\partial t}dm \tag{A9b}$$

$$= -4\frac{GM\dot{M}}{R} - 3\int_{M_c}^{M}\frac{\partial P}{\partial t}\frac{dm}{\rho} + 3V_M\frac{\partial P_M}{\partial t} - 3V_c\frac{\partial P_c}{\partial t} \tag{A9c}$$

where Equations (A9b) and (A9c) use hydrostatic balance and integration by parts.

Subtracting Equations (A5) and (A9c) and rearranging terms with the help of Equations (A2), (A3) and (A4) gives

$$\int_{M_c}^{M}\frac{P}{\rho^2}\frac{\partial \rho}{\partial t}dm = -\dot{E}_G - \frac{GM\dot{M}}{R} - P_M\frac{\partial V_M}{\partial t} . \tag{A10}$$

Combining Equations (A1c), (A5) and (A10), we reproduce Equation (17) with the accreted specific energy $e_M \equiv u_M - GM/R$.

B. ANALYTIC COOLING MODEL DETAILS

TODO (academic): Figure out if theta ¡ 1 is actually required? Should be but need to check